bioRxiv preprint doi: https://doi.org/10.1101/2020.07.07.191320; this version posted July 8, 2020. The copyright holder for this preprint (which was not certified by peer review) is the author/funder, who has granted bioRxiv a license to display the preprint in perpetuity. It is made available under a CC-BY-NC-ND 4.0 International license.

Reduced phenotypic plasticity evolves in less predictable environments

Christelle Leung[1], Marie Rescan[1], Daphné Grulois[1] & Luis-Miguel Chevin[1]

[1] CEFE, Université de Montpellier, CNRS, EPHE, IRD, Université Paul Valéry Montpellier 3, Montpellier, France.

Christelle Leung: https://orcid.org/0000-0002-7242-3075; christelle.leung@umontreal.ca

Marie Rescan: https://orcid.org/0000-0001-8484-5948; marie.rescan@cefe.cnrs.fr

Daphné Grulois: https://orcid.org/0000-0002-3054-1364; daphne.grulois@cefe.cnrs.fr

Luis-Miguel Chevin: https://orcid.org/0000-0003-4188-4618; luis-migel.chevin@cefe.cnrs.fr

Short running title: Unpredictable environments reduce plasticity

Keywords: Phenotypic plasticity, experimental evolution, fluctuating environment, environmental stochasticity, predictability, *Dunaliella salina*.

***Corresponding Author:**

Christelle Leung or Luis-Miguel Chevin

Centre d'Écologie Fonctionnelle et Évolutive

1919 route de Mende

34293 Montpellier Cedex 5, France

+33 (0)4 67 61 32 11

christelle.leung@umontrea.ca or luis-miguel.chevin@cefe.cnrs.fr

bioRxiv preprint doi: https://doi.org/10.1101/2020.07.07.191320; this version posted July 8, 2020. The copyright holder for this preprint (which was not certified by peer review) is the author/funder, who has granted bioRxiv a license to display the preprint in perpetuity. It is made available under a CC-BY-NC-ND 4.0 International license.

Abstract

Phenotypic plasticity is a prominent mechanism for coping with variable environments, and a key determinant of extinction risk. Evolutionary theory predicts that phenotypic plasticity should evolve to lower levels in environments that fluctuate less predictably, because they induce mismatches between plastic responses and selective pressures. However this prediction is difficult to test in nature, where environmental predictability is not controlled. Here, we exposed 32 lines of the halotolerant microalga *Dunaliella salina* to ecologically realistic, randomly fluctuating salinity, with varying levels of predictability, for 500 generations. We found that morphological plasticity evolved to lower levels in lines that experienced less predictable environments. Evolution of plasticity mostly concerned phases with slow population growth, rather than the exponential phase where microbes are typically phenotyped. This study underlines that long-term experiments with complex patterns of environmental change are needed to test theories about population responses to altered environmental predictability, as currently observed under climate change.

Introduction

Phenotypic plasticity, the ability of a given genotype to produce alternative phenotypes depending on its environment of development or expression, is a major mechanism for responding to environmental variation across the tree of life (Scheiner 1993; Schlichting & Pigliucci 1998; West-Eberhard 2003). In recent years, the study of phenotypic plasticity has gained prominence in evolutionary ecology, with the realization that it contributes a substantial part to observed phenotypic change in the wild, notably in response to climate change (Gienapp *et al.* 2008; Merilä & Hendry 2014). Because phenotypic change is generally a strong determinant of population dynamics (Pelletier *et al.* 2007; Ozgul *et al.* 2010; Ellner *et al.* 2011), this implies that phenotypic plasticity can strongly impact population growth and extinction risk in a rapidly changing world, to an extent that depends on the rate and pattern of environmental change (Chevin *et al.* 2010; Reed *et al.* 2010; Chevin *et al.* 2013b; Vedder *et al.* 2013; Ashander *et al.* 2016; Phillimore *et al.* 2016).

bioRxiv preprint doi: https://doi.org/10.1101/2020.07.07.191320; this version posted July 8, 2020. The copyright holder for this preprint (which was not certified by peer review) is the author/funder, who has granted bioRxiv a license to display the preprint in perpetuity. It is made available under a CC-BY-NC-ND 4.0 International license.

However, despite the ubiquity and ecological importance of phenotypic plasticity, proving its adaptiveness for any particular trait and organism is particularly challenging (Ghalambor *et al.* 2007). Most evidence that plasticity is adaptive is instead indirect, for instance through comparison of the direction of plastic *vs* evolved responses to a novel environment (Ghalambor *et al.* 2015), except for rare studies where plastic responses have been genetically engineered to compare the fitness of plastic *vs* non-plastic genotypes across environments (Dudley & Schmitt 1996). However, beyond the putative advantage of being plastic, a more meaningful and quantitative question is whether a given degree of plasticity is adaptive. This question was thoroughly addressed theoretically, and the predictability of environmental variation was identified as a key determinant of the adaptiveness of plasticity, and driver of its long-term evolution (Gavrilets & Scheiner 1993; de Jong 1999; Lande 2009; Reed *et al.* 2010; Botero *et al.* 2015; Tufto 2015). In particular, theory predicts that phenotypic plasticity should evolve to lower levels in environments that fluctuate less predictably, because this leads to plastic responses that do not match future selective pressures (Gavrilets & Scheiner 1993; de Jong 1999; Lande 2009; Botero *et al.* 2015; Tufto 2015). Nevertheless, these predictions still largely lack direct empirical evidence (but see Scheiner & Yampolsky 1998; Dey *et al.* 2016), owing to the difficulty in manipulating the variability and predictability of the environment over evolutionary times. In addition, multiple independent replicates of environmental fluctuations are needed in order to account for their inherent randomness (environmental stochasticity), but this is difficult to achieve in nature.

A useful alternative to circumvent these limitations is to perform long-term laboratory experiments under controlled, yet ecologically realistic, patterns of environmental fluctuations. This approach, which was previously advocated by Chevin *et al.* (2013a), allows controlling for the level of environmental predictability, with all other things being equal - including the mean and variance of the environment -, and also permits sufficiently large duration and replication to unambiguously observe evolutionary responses to stochastic environments. Here we have applied this approach with the unicellular microalga *Dunaliella salina*, the main primary producer in hypersaline environments such as continental salt lakes, coastal lagoons, and salterns (Oren 2005; Ben-Amotz *et al.* 2009). The cell shape and content of this microalgae are known to respond plastically to salinity over different timescales, allowing for both immediate morphological responses to sudden osmotic stress, and slower

bioRxiv preprint doi: https://doi.org/10.1101/2020.07.07.191320; this version posted July 8, 2020. The copyright holder for this preprint (which was not certified by peer review) is the author/funder, who has granted bioRxiv a license to display the preprint in perpetuity. It is made available under a CC-BY-NC-ND 4.0 International license.

83 physiological adjustments involving the production of metabolites (glycerol, carotene) inside
84 the cell (Oren 2005; Ben-Amotz *et al.* 2009). Several of these traits can be measured at the
85 individual level and at high-throughput, pushing work on phenotypic plasticity towards the
86 realm of phenomics (Houle *et al.* 2010; Pendergrass *et al.* 2013; Yvert *et al.* 2013).
87 Experimental evolution has been successfully performed previously with the closely related
88 species *Dunaliella tertiolecta* (Malerba *et al.* 2018). Furthermore, we have recently shown
89 that phenotypic plasticity plays a crucial role in the population dynamics and extinction risk
90 of *Dunaliella salina* in a randomly fluctuating environment (Rescan *et al.* 2020). This makes
91 *D. salina* particularly well-suited to investigate experimentally the evolution of phenotypic
92 plasticity in response to environmental predictability.

93

94 **Material and Methods**

95 **Experimental evolution**

96 We followed up on the experimental evolution protocol initiated by Rescan *et al.* (2020),
97 which we pursued for several hundred generations. Briefly, we used two genetically related
98 strains (CCAP 19/12 and CCAP 19/15) of the halophilic unicellular microalga *Dunaliella*
99 *salina*, which can tolerate a broad range of salinities. Long-term experimental evolution
100 occurred from August 2017 to January 2019, during which we exposed 32 populations to
101 randomly fluctuating salinity, and 4 populations to a constant intermediate salinity ([NaCl] =
102 2.4 M). Salinity changes occurred twice a week, by 20% dilution into 800 µl of fresh medium
103 to account for population extinction (Rescan *et al.* 2020), using a liquid-handling robot
104 (Biomek NXP Span-8; Beckman Coulter). At each transfer, the target salinity was achieved
105 by mixing the required volumes of hypo- ([NaCl] = 0M) and hyper- ([NaCl] = 4.8M) saline
106 media, after accounting for dilution of the pre-transfer salinity (Rescan *et al.* 2020). We
107 totalized at least 139 salinity transfers and more than 500 generations (assuming ~1
108 generation per day (Ben-Amotz *et al.* 2009)). The populations in fluctuating environments
109 were subjected to independent random time series over a continuous range (first-order
110 autoregressive process, AR1), rather than a more artificial alternation of low vs high salinity
111 treatments. All the lines had the same long-term stationary mean (μ = 2.4M [NaCl]) and
112 variance (σ = 1) of salinity, but they differed in how salinity at a given time depends on the

bioRxiv preprint doi: https://doi.org/10.1101/2020.07.07.191320; this version posted July 8, 2020. The copyright holder for this preprint (which was not certified by peer review) is the author/funder, who has granted bioRxiv a license to display the preprint in perpetuity. It is made available under a CC-BY-NC-ND 4.0 International license.

previous salinity, prior the last transfer, as determined by the temporal autocorrelation ρ of salinity (Fig. 1A & Fig. 1B) (Rescan *et al.* 2020). The predictability of environmental change upon these transfers depended on ρ^2, the proportion of the temporal variance in salinity explained by the previous salinity (Fig. 1B). There were four autocorrelation treatments, for which the expected autocorrelations (over infinite time) were $\bar{\rho}$ = -0.5, 0, 0.5, and 0.9 (Fig. 1; see Rescan *et al.* (2020) for detailed protocol), but the realized autocorrelation over the duration of the experiment spanned a continuum of values. All populations were cultivated in 1.1ml of 96-deepwell plates (Axygen®; Corning Life Sciences) in an artificial seawater prepared as described in Rescan *et al.* (2020), at constant temperature (24°C) and 12/12 lighting (200 µmol.m^{-2}.s^{-1}).

At the end of the experiment, we genetically confirmed that strains were not cross-contaminated after ~1.5 year of experiment. Specifically, for each evolved lines, we amplified one mitochondrial (333 pb fragment using the primers DsMt1-For [5'-GGTTAGTCATAGTTGGAGGT-3'] and DsMt1_-Rev [5'-GAAAACCTAACATGGCTAAGC-3'] and chloroplast (372 bp fragment using the primers DsChl1-For [5'-TTTAGGCGAATCCATAAGAG-3'] and DsChl1-Rev [5'-CCAAGCAGGTGAATTAGCTTTG-3']) locus, specific to CCAP 19/12 and CCAP 19/15, respectively.

Phenotypic plasticity assays

To assess the plasticity degree of the 36 evolved lineages, we compared individual cell morphologies between two salinities near the extremes of their historical range ([NaCl] = 0.8M and 4.0M). These lineages started with potentially genetically diverse strains, and were certainly also polymorphic at the end of experimental evolution. To verify that morphological changes between salinities over the 10-day assay were due to plastic responses rather than environment-specific selection, we also performed the phenotypic plasticity assays with 20 additional isogenic populations derived from five heterogenic experimental lines. One of these experimental lines was the CCAP 19/12 strain that evolved in constant salinity (2.4 M) and four others were from the CCAP 19/15 strain that evolved in constant (2.4 M) and fluctuating (with targeted autocorrelation ρ = -0.5, ρ = 0 and ρ = 0.9) salinities. For each of these five experimental populations, we founded four different population from single cells

bioRxiv preprint doi: https://doi.org/10.1101/2020.07.07.191320; this version posted July 8, 2020. The copyright holder for this preprint (which was not certified by peer review) is the author/funder, who has granted bioRxiv a license to display the preprint in perpetuity. It is made available under a CC-BY-NC-ND 4.0 International license.

143 isolated using cells-sorting flow cytometry (BD *FACSAria*™ IIu ; Biosciences-US). Because
144 *Dunaliella salina* is haploid, we expected all cells to be genetically identical in populations
145 founded from a single one.

146 The 36 lines were sampled from different salinities and at different population sizes at
147 the end of the evolutionary experiment (Rescan *et al.* 2020). To ensure that all cells were in
148 similar physiological states and at similar population densities at the beginning of the
149 phenotypic plasticity assay, we first acclimated them for 10 days in the same environmental
150 conditions. We transferred 400 µl of each experimental population into 50 ml flasks
151 (CellStar®; Greiner BioOne) with 25 ml of fresh medium at salinity [NaCl] = 2.4 M,
152 temperature 24°C, and light intensity 200 µmol m^{-2} s^{-1} for 12:12 h light/dark cycles.

153 Following the acclimation step, we inoculated ~2 × 10^4 cells.ml^{-1} of each population
154 into low (0.8 M) and high (4.0 M) salinity medium (Fig. 1), to track their population density
155 and morphological traits for 10 days. For 24 populations (including 14 randomly chosen
156 evolved lines and 10 isogenic populations), we also inoculated the same number of cells into
157 2.4 M salinity medium to assess morphological changes independent from salinity changes.
158 We randomly placed all conditions in 2 ml 96-deepwell plates at 24°C and 12/12 lighting.

159 When placed in a new salinity, *D. salina* undergoes changes in cell shape and content,
160 reflecting an osmotic adaptability that unfolds over different timescales (Ben-Amotz *et al.*
161 2009). Rapid changes in cell volume in response to changes in extracellular osmolarity are
162 made possible by lack of a rigid cell wall. This then triggers longer physiological responses
163 involving the production of osmolites (especially glycerol), changes in gene expression, and
164 the production of diverse salt-induced proteins (Azachi *et al.* 2002; Oren 2005; Ben-Amotz *et*
165 *al.* 2009), which all modify the cell content. To assess the changes in cell morphology, we
166 passed a 150 µL sample of each population through flow cytometry at 11 time points: at the
167 end of the acclimation step (day = 0), 4h after environmental changes (day = 1), and once per
168 day from day = 2 to day = 10.

169 Intrinsic structural parameters of cells were measured using a Guava® EasyCyte™ HT
170 cytometer (Luminex Corporation, Texas, USA) with a laser emitting at 488 nm. The
171 cytometer was calibrated each day of the experiment using the Guava® EasyCheck™ kit, and
172 settings were adjusted before each measurement. The flow rate was set to 1.18 µl.s^{-1}, for 30s

bioRxiv preprint doi: https://doi.org/10.1101/2020.07.07.191320; this version posted July 8, 2020. The copyright holder for this preprint (which was not certified by peer review) is the author/funder, who has granted bioRxiv a license to display the preprint in perpetuity. It is made available under a CC-BY-NC-ND 4.0 International license.

or until the number of counted events reached 5,000. Data processing was carried out using Guava® InCyte Software version 3.3, from which we exported list-mode data files of measurements on the logarithmic scale. Non-algal particles and dead algae were excluded from the analysis according a cytogram of emissions at Red-B (695/50 nm) and Yellow-B (583/26 nm) band pass filters, enabling a clear discrimination between algae populations and other events thanks to chlorophyll auto-fluorescence (Rescan *et al.* 2020). We also discriminated doublets (i.e. single events that actually consists of two independent cells) from singlets according to the width of the electronic pulse measurement (FSC-W) (Wersto *et al.* 2001). For events categorized as single alive *D. salina* cells, we specifically assessed the environment-specific cell morphology using the Forward Scatter (FSC), Side Scatter (SSC) and fluorescence emission at 695/50 nm band pass filter (Red-B) values as proxy for cells size, complexity (granularity, cytoplasmic contents) (Adan *et al.* 2017), and chlorophyll production (Papageorgiou 2004), respectively. The density of the medium is likely to alter the light signal. To control for this effect, we subtracted from each individual measurement of FSC, SSC and Red-B the mean value of the same parameter values among 1,000 Guava® EasyCheck™ calibrating beads placed in artificial seawater at the same salinity ([NaCl] = 0.8 M, 2.4 M or 4.0 M). We confirmed that traits we measured using FCM closely matched cell size, shape and cellular contents including chlorophyll production, as there was 90.06% ($P < 0.001$) correspondence between PCAs performed with data from FCM vs image processing of epifluorescence microscopy (Procrustes analysis; Supp. Fig. S1). Finally, for each days and salinity, we determined population densities from the ratio of the count of events identified as alive *D. salina* cells to the total volume of acquisition.

Statistical analyses

Population dynamics

For each population and salinity, we calculated the *per-capita* growth rate of the population per day during the phenotypic plasticity assay, as $r = \frac{N(t) - N(t-1)}{N(t)}$, where N is the population density (cells × ml^{-1}), and t a time point of measurement (in days). For $N(0)$, we used the initial density of 2×10^4 cells.ml^{-1} that we inoculated in each environment following the acclimation step. We describe days when r is highest as the exponential growth phase, while

bioRxiv preprint doi: https://doi.org/10.1101/2020.07.07.191320; this version posted July 8, 2020. The copyright holder for this preprint (which was not certified by peer review) is the author/funder, who has granted bioRxiv a license to display the preprint in perpetuity. It is made available under a CC-BY-NC-ND 4.0 International license.

with slower positive growth rates before and after the exponential phase are described as lag and stationary phases, respectively.

Morphological variation and dynamics

Flow cytometry allows analyzing thousands of individual cells in seconds, achieving high-throughput phenotyping. Here, the low population density following transfer to a new environment (Days 1-2) limited the number of cells that could be measured by the flow cytometer, accounting for our measurement parameters. To keep a balanced design, we therefore randomly selected up to 150 events categorized as alive *D. salina* per conditions – i.e. population, environment and day –, totalizing more than 2×10^5 individual cells for this study.

We then used a multivariate approach based on Redundancy Analyses (RDA) (Borcard *et al.* 1992) to assess the proportion of morphological variation explained by different predictors. For each *D. salina* cell, we used the morphological measurements (FSC, SSC and Red-B cytometer values) as the multivariate response variable, and ancestral strain identity (CCAP 19/12 or CCAP 19/15), salinity during the plasticity assay, time point of measurement (day), and associated *per-capita* growth rate, as explanatory variables. Variation partitioning was performed separately for populations that evolved in fluctuating *vs* constant environments. For populations that evolved in fluctuating environments, the predictability of environmental change during long-term evolution was included as an additional explanatory variable. As mentioned above, different time series within an autocorrelation treatment may vary in their realized autocorrelation, because of the randomness of the stochastic process in finite time. We therefore computed the realized environmental autocorrelation ρ as the correlation between salinities at two subsequent transfers, throughout each salinity time series. We then assessed the environmental predictability as ρ^2, and used it as a continuous explanatory variable.

We quantified the effects of all explanatory factors or variables and their interactions through their contributions to total variation using a multivariate version of R^2, and tested the significance of each R^2 by ANOVA-like permutation tests, using 999 randomizations of the data (Borcard *et al.* 1992; Legendre & Legendre 1998; Peres-Neto *et al.* 2006). A significant *salinity* × *predictability* interaction characterized the evolution of plasticity in response to our

bioRxiv preprint doi: https://doi.org/10.1101/2020.07.07.191320; this version posted July 8, 2020. The copyright holder for this preprint (which was not certified by peer review) is the author/funder, who has granted bioRxiv a license to display the preprint in perpetuity. It is made available under a CC-BY-NC-ND 4.0 International license.

232 predictability treatment, a significant *day* × *salinity* interaction characterized a salinity-
233 specific ontogenic trajectory of morphology, and a significant three wise *day* × *salinity* ×
234 *predictability* interaction indicated that the evolution of plasticity had different effects at
235 different days along the ontogenic trajectory.

236 To illustrate the temporal changes in cells morphology following osmotic stress, we
237 represented the mean cell morphology for each day in a morphospace for each targeted
238 autocorrelation ($\bar{\rho}$). To do so, we first performed a Principal Component Analysis (PCA) of
239 the morphological measurements of the entire dataset, and calculated the centroid for each
240 conditions (i.e. for a given salinity, day and population). We then represented the mean
241 morphology with their standard errors, per day and salinity, by averaging over all populations
242 for each targeted $\bar{\rho}$, and represented them along the two first PCA axes (Fig. 3B).

243 *Evolution of the degree of plasticity*

244 To assess how the magnitude of phenotypic plasticity evolved in our experiment, we first
245 computed the Euclidian distance between the centroids (multivariate means) of each
246 experimental population measured at high (4M) *vs* low (0.8M) salinity. We then compared
247 this degree of plasticity among the experimental populations, to test whether it evolved
248 according to environmental predictability. Specifically, for each day following transfer to the
249 new salinity, we regressed the Euclidian distance of plastic change against ρ^2, as index for
250 environmental predictability. The significance of this regression was assessed by hierarchical
251 non-parametric bootstrapping. We first resampled with replacement 32 populations among the
252 32 populations that evolved in fluctuating environments. For each population in each salinity,
253 we resampled $n = 150$ cells with replacement. We then recomputed the degrees of plasticity of
254 all populations, and regressed them against ρ^2, iterating the full process 1,000 times. The
255 proportion of simulations with slopes larger than 0 was used to assess the significance of the
256 evolution of lower plasticity in populations evolved in less predictable environments.

257 We performed all statistical analyses in the environment R version 3.5.3 (R Core
258 Team 2019) with the vegan package version 2.5-4 (Oksanen *et al.* 2019) for the multivariate
259 analyses.

260

bioRxiv preprint doi: https://doi.org/10.1101/2020.07.07.191320; this version posted July 8, 2020. The copyright holder for this preprint (which was not certified by peer review) is the author/funder, who has granted bioRxiv a license to display the preprint in perpetuity. It is made available under a CC-BY-NC-ND 4.0 International license.

Results

Evolution of reduced plasticity

We first investigated the plasticity of cells that had approached phenotypic equilibrium, 10 days after transfer to a new salinity. Comparison of samples from low *vs* high salinities revealed a clear signal of plasticity, with a significant effect of salt concentration on cell morphology (Table 1). Cells from high salinity were smaller and contained less chlorophyll than cells from low salinity (Fig. 2A & Supp. Fig. S2A). However this plasticity was not identical in all experimental lines: those that evolved in different environmental predictabilities differed in their plastic responses to salinity (Fig. 2B; significant *salinity* × ρ^2 interaction in Table 1). The magnitude of plasticity, as quantified by the Euclidian distance of phenotypic change between low and high salinities (length of black segments in Fig. 2B, & Supp. Fig. S2B), was positively correlated to the environmental predictability during experimental evolution, with lines from less predictable environments displaying reduced plasticity (linear regression: $R^2 = 0.621$, $P < 0.001$; Fig. 2C). This result was replicated over the two ancestral strains (Fig. 2C) despite their differences on other features such as their population dynamics (Fig. 3A & Supp. Fig. S3), and also held for isogenic populations (Fig. S4A). The latter confirmed that the observed morphological differences between salinities were the result of phenotypic plasticity, rather than rapid selection of salinity-specific genotypes over the assay experiment (since isogenic populations display no genetic variation).

We also maintained four lines at constant salinity ([NaCl] = 2.4M) throughout the experiment, as controls for the influence of environmental fluctuations. Lines that evolved in constant environments (right panel in Fig. 2C & Supp. Fig. S4A) had a similar degree of plasticity as lines evolved under highly predictable environmental fluctuations ($P = 0.295$). This suggests that unpredictable environments exerted a stronger selective pressure against plasticity (Gavrilets & Scheiner 1993; Lande 2009) than any putative cost associated to the maintenance of plasticity in a constant environment (DeWitt *et al.* 1998). Interestingly, we found similar degrees of plasticity between populations that evolved in treatments with autocorrelations $\bar{\rho} = -0.5$ and $\bar{\rho} = 0.5$ ($P = 0.867$), which have the same expected predictability of changes ($\rho^2 = 0.25$), but different magnitude of transitions upon each transfer (Supp. Fig. S5).

bioRxiv preprint doi: https://doi.org/10.1101/2020.07.07.191320; this version posted July 8, 2020. The copyright holder for this preprint (which was not certified by peer review) is the author/funder, who has granted bioRxiv a license to display the preprint in perpetuity. It is made available under a CC-BY-NC-ND 4.0 International license.

Ontogeny of evolved plasticity

We then turned to the entire morphological trajectory over 10 days, to investigate how the evolution of plasticity unfolds along developmental time scales. When cells were transferred at low density (~2 × 10^4 cells.ml^{-1}) to fresh medium with unchanged salinity, their morphology followed a loop-shaped trajectory over 10 days, with initial and final phenotypes markedly differing from phenotypes at intermediate times (Fig. 3A). These changes concerned cell size and granularity for the first days (up to days 2-3: bigger cells when reaching the exponential phase), followed by changes in chlorophyll content (days 3-4 to 10: decreasing chlorophyll content in the stationary phase) (Fig. 3A-B & Supp. Fig. S1A). As this temporal trend in morphology was also found for isogenic populations with effectively no opportunity for natural selection (Fig. 3A-B), it does not reflect genetic changes in the population. Instead, these changes can be described as ontogenic, in line with the extended definition of ontogeny/development as a sequence of cellular states, applying across unicellular and multicellular organisms (Gilbert 2000). Part of this ontogenic morphological variation was explained by population growth rate (Table 1), an aggregate population-level outcome of life-history traits of individual cells (division and death rate), which is typically used as an indicator of physiological state in microbiology (Maharjan *et al.* 2013). Focusing on populations maintained in the same salinity as during acclimation ([NaCl] = 2.4 M), we detected a clear effect of growth rate (R^2 = 0.046, P < 0.001) on morphological variation (red arrow in Fig. 3A; same effect for both ancestral strains, *growth rate* × *strain* interaction: P = 0.504), independent from salinity changes. However, the population growth rate was not sufficient to explain the ontogenic trajectory, and there remained a significant marginal effect of the time spent in the new environment (R^2 = 0.031, P < 0.001).

Ontogenic trajectories also differed between salinities. Upon transfer to a new salinity, morphologies in the hypo- *vs* hyper-osmotic environments first rapidly diverged in opposite directions from the acclimated morphology, 4h after salinity change (day 1 in green and yellow vs red dot; Fig. 3B), before converging during the exponential phase, and finally diverging again to salinity-specific morphologies over the stationary phase (Fig. 3B & Supp. Fig. S2A). This is consistent with known responses of *D. salina* to salinity change, which first involve an immediate – sometimes drastic – change in cell volume caused by water intake/loss, followed by slower accumulation of salt-induced proteins and metabolites

bioRxiv preprint doi: https://doi.org/10.1101/2020.07.07.191320; this version posted July 8, 2020. The copyright holder for this preprint (which was not certified by peer review) is the author/funder, who has granted bioRxiv a license to display the preprint in perpetuity. It is made available under a CC-BY-NC-ND 4.0 International license.

(notably via changes in gene expression (Chen & Jiang 2009; Fang *et al.* 2017)), which restore cell shape and eventually leads to long-term changes in cell content such as lipid, carotene, and glycerol accumulation (Ben-Amotz *et al.* 2009). As a result of these differences in morphological trajectories between salinities, the plasticity of cell morphology was temporally variable (significant *day* × *salinity* interaction; Table 1). Plastic differences in morphology also followed a loop over 10 days, where initial and final differences diverged from those at intermediate times (Supp. Fig. S2B). The degree of plasticity was highest at low population growth rates characteristic of the lag and stationary phases, and lowest during the exponential phase (significant *salinity* × *growth rate* interaction, Table 1, Fig. 3C-E and Supp. Fig. S2).

Evolution of plasticity in response to environmental predictability had different impacts at distinct stages of the ontogenic trajectory. We found a positive relationship between the level of plasticity and environmental predictability during phases of slow population growth (at day 2, and from days 6 to 10; Fig. 3C-E), but no relationship at day 1 and during the exponential phase (days 3 to 4; Fig. 3C-E; similar results were observed for isogenic populations, Supp. Fig. S4B). That there was little evolution of plasticity during the exponential phase is consistent with the finding that morphological plasticity is generally lowest in this phase (Fig. 3C-D). In contrast, plasticity is high shortly after salinity transfer (day 1, Fig. 3D), but mostly because of passive, reflex responses to osmotic stress, which are certainly less prone to evolution than longer term physiological responses involving specific gene expression and production of metabolites and chlorophyll.

Discussion

We have shown that phenotypic plasticity, a major component of phenotypic change in the wild (Scheiner 1993; Schlichting & Pigliucci 1998; West-Eberhard 2003; Pelletier *et al.* 2007; Ozgul *et al.* 2010; Ellner *et al.* 2011), and a key mechanism for population persistence in a changing environment (Chevin *et al.* 2010; Reed *et al.* 2010; Chevin *et al.* 2013b; Vedder *et al.* 2013; Ashander *et al.* 2016; Phillimore *et al.* 2016), can evolve experimentally in response to environmental predictability, in the direction predicted by theory (Gavrilets & Scheiner 1993; de Jong 1999; Lande 2009; Botero *et al.* 2015; Tufto 2015). This plasticity concerned morphological traits that were previously described to be involved in salinity tolerance in

bioRxiv preprint doi: https://doi.org/10.1101/2020.07.07.191320; this version posted July 8, 2020. The copyright holder for this preprint (which was not certified by peer review) is the author/funder, who has granted bioRxiv a license to display the preprint in perpetuity. It is made available under a CC-BY-NC-ND 4.0 International license.

352 *Dunaliella salina* (Azachi *et al.* 2002; Oren 2005; Ben-Amotz *et al.* 2009), a species for
353 which we have shown that plastic responses to past environments can largely drive population
354 dynamics and extinction risk in a randomly fluctuating environment (Rescan *et al.* 2020).

355 Contrary to common practice in experimental evolution with microbes (Elena &
356 Lenski 2003; Buckling *et al.* 2009), we have assayed evolved changes by measuring multiple
357 individual traits (rather than aggregate population traits) across environments and over time.
358 This approach, tending towards phenomics, allowed us to describe an ontogenic sequence of
359 cell morphology, consistent with osmotic response mechanisms operating at different time
360 scales. These responses ranged from immediate physical change in cell shape (passive
361 plasticity) occurring within the first few seconds/minutes, to long-term physiological
362 regulations involving changes in gene expression (active plasticity), which usually start within
363 12–24h (Chen & Jiang 2009; Fang *et al.* 2017). These consecutive morphological states of
364 cells, which we here described as an ontogenic sequence (Gilbert 2000), can also be
365 interpreted as alternative phenotypes favored at different population densities (*r* vs *K*-
366 selection (MacArthur 1962; Sæther *et al.* 2016)), or plastic responses to environmental
367 variables other than salinity that change along time in a batch culture (e.g. resource abundance
368 and quality) (Collot *et al.* 2018).

369 Evolution of active plasticity in response to environmental predictability was
370 essentially restricted to physiological states associated with phases of slow – or even null –
371 population growth in our experiment. Population growth status, indicative of the
372 physiological state of individual cells, is known to be associated with multiple phenotypic
373 traits micro-organisms (Maharjan *et al.* 2013). The lack of plasticity during the exponential
374 phase likely results from a particular morphology associated to rapid cell division, which
375 masks the influence of salinity. However, the late expression (day 5-10) of morphological
376 changes that we observed in response to osmotic stress was initiated as soon as the start of the
377 active plasticity (day 2). Similarly, we also observed the evolution of reduced plasticity
378 according to environmental predictability as early as the beginning of the ontogenic sequence
379 of cells morphology.

380 Our results demonstrate that long-term experimental evolution under complex,
381 ecologically realistic patterns of environmental variation, coupled with intense high-

bioRxiv preprint doi: https://doi.org/10.1101/2020.07.07.191320; this version posted July 8, 2020. The copyright holder for this preprint (which was not certified by peer review) is the author/funder, who has granted bioRxiv a license to display the preprint in perpetuity. It is made available under a CC-BY-NC-ND 4.0 International license.

throughput phenotyping at the individual level, allows testing fundamental predictions in evolutionary ecology that are barely approachable in natural settings. Our finding that phenotypic plasticity can evolve in response to environmental predictability proves important for the prospects for population persistence in the face of global warming, and other anthropogenic changes. Indeed these changes consist not only of trends in mean environments, but also alterations in the magnitude and predictability of natural environmental fluctuations (Wigley *et al.* 1998; Boer 2009). Theoretical work has made it clear that phenotypic plasticity can strongly influence extinction risk in response to changing environmental predictability (Reed *et al.* 2010; Chevin *et al.* 2013a; Botero *et al.* 2015; Ashander *et al.* 2016), which was recently confirmed empirically using laboratory experiments (Proulx *et al.* 2019; Rescan *et al.* 2020). In particular, this theory has shown that evolution of lower phenotypic plasticity can reduce extinction risk under reduced environmental predictability, by decreasing the magnitude of mismatches between the population mean phenotype and the optimum phenotype determined by the environment (Chevin *et al.* 2013a; Ashander *et al.* 2016). Our demonstration that such evolution of reduced plasticity can indeed occur over a few hundred generations indicate that this may be an important mechanism by which species may persist under climate change.

Acknowledgements

We are grateful to S. Bedhomme, P. Nosil and R. Villoutreix for comments on an earlier version of the manuscript. We thank the MRI-IGMM and MRI-CRBM platforms (Montpellier) for access to the cell sorter and microscopy, respectively. This work was supported by the European Research Council (Grant 678140-FluctEvol) to L-MC, and a Fonds de Recherche du Québec - Nature et Technologies (FRQNT) fellowship to CL.

Competing interest

Authors declare no competing interests.

bioRxiv preprint doi: https://doi.org/10.1101/2020.07.07.191320; this version posted July 8, 2020. The copyright holder for this preprint (which was not certified by peer review) is the author/funder, who has granted bioRxiv a license to display the preprint in perpetuity. It is made available under a CC-BY-NC-ND 4.0 International license.

Supplementary Information

Supplementary information include Supplementary Material 1, and Supplementary figures S1 to S5.

References

Adan, A., Alizada, G., Kiraz, Y., Baran, Y. & Nalbant, A. (2017). Flow cytometry: Basic principles and applications. *Crit. Rev. Biotechnol.*, 37, 163-176.

Ashander, J., Chevin, L.-M. & Baskett, M.L. (2016). Predicting evolutionary rescue via evolving plasticity in stochastic environments. *Proc. R. Soc. B*, 283, 20161690.

Azachi, M., Sadka, A., Fisher, M., Goldshlag, P., Gokhman, I. & Zamir, A. (2002). Salt induction of fatty acid elongase and membrane lipid modifications in the extreme halotolerant alga *Dunaliella salina*. *Plant Physiol.*, 129, 1320-1329.

Ben-Amotz, A., Polle, J.E.W. & Subba, R.D.V. (2009). *The alga Dunaliella: Biodiversity, physiology, genomics and biotechnology.* Science Publishers, Enfield, NH.

Boer, G. (2009). Changes in interannual variability and decadal potential predictability under global warming. *J. Clim.*, 22, 3098-3109.

Borcard, D., Legendre, P. & Drapeau, P. (1992). Partialling out the spatial component of ecological variation. *Ecology*, 73, 1045-1055.

Botero, C.A., Weissing, F.J., Wright, J. & Rubenstein, D.R. (2015). Evolutionary tipping points in the capacity to adapt to environmental change. *Proc. Natl. Acad. Sci. U.S.A.*, 112, 184-189.

Buckling, A., Maclean, R.C., Brockhurst, M.A. & Colegrave, N. (2009). The Beagle in a bottle. *Nature*, 457, 824-829.

Chen, H. & Jiang, J.G. (2009). Osmotic responses of *Dunaliella* to the changes of salinity. *Journal of Cellular Physiology*, 219, 251-258.

Chevin, L.-M., Gallet, R., Gomulkiewicz, R., Holt, R.D. & Fellous, S. (2013a). Phenotypic plasticity in evolutionary rescue experiments. *Phil. Trans. R. Soc. B*, 368, 20120089.

bioRxiv preprint doi: https://doi.org/10.1101/2020.07.07.191320; this version posted July 8, 2020. The copyright holder for this preprint (which was not certified by peer review) is the author/funder, who has granted bioRxiv a license to display the preprint in perpetuity. It is made available under a CC-BY-NC-ND 4.0 International license.

437 Chevin, L.-M., Lande, R. & Mace, G.M. (2010). Adaptation, plasticity, and extinction in a
438 changing environment: towards a predictive theory. *PLoS Biol.*, 8, e1000357.

439 Chevin, L.M., Collins, S. & Lefèvre, F. (2013b). Phenotypic plasticity and evolutionary
440 demographic responses to climate change: Taking theory out to the field. *Funct. Ecol.*,
441 27, 967-979.

442 Collot, D., Nidelet, T., Ramsayer, J., Martin, O.C., Méléard, S., Dillmann, C. *et al.* (2018).
443 Feedback between environment and traits under selection in a seasonal environment:
444 consequences for experimental evolution. *Proc. R. Soc. B*, 285, 20180284.

445 de Jong, G. (1999). Unpredictable selection in a structured population leads to local genetic
446 differentiation in evolved reaction norms. *J. Evol. Biol.*, 12, 839-851.

447 DeWitt, T.J., Sih, A. & Wilson, D.S. (1998). Costs and limits of phenotypic plasticity. *Trends*
448 *Ecol. Evol.*, 13, 77-81.

449 Dey, S., Proulx, S.R. & Teotonio, H. (2016). Adaptation to temporally fluctuating
450 environments by the evolution of maternal effects. *PLoS Biol.*, 14, e1002388.

451 Dudley, S.A. & Schmitt, J. (1996). Testing the adaptive plasticity hypothesis: density-
452 dependent selection on manipulated stem length in *Impatiens capensis*. *The American*
453 *Naturalist*, 147, 445-465.

454 Elena, S.F. & Lenski, R.E. (2003). Evolution experiments with microorganisms: the dynamics
455 and genetic bases of adaptation. *Nature Reviews Genetics*, 4, 457-469.

456 Ellner, S.P., Geber, M.A. & Hairston Jr, N.G. (2011). Does rapid evolution matter?
457 Measuring the rate of contemporary evolution and its impacts on ecological dynamics.
458 *Ecol. Lett.*, 14, 603-614.

459 Fang, L., Qi, S., Xu, Z., Wang, W., He, J., Chen, X. *et al.* (2017). De novo transcriptomic
460 profiling of *Dunaliella salina* reveals concordant flows of glycerol metabolic
461 pathways upon reciprocal salinity changes. *Algal Research*, 23, 135-149.

462 Gavrilets, S. & Scheiner, S.M. (1993). The genetics of phenotypic plasticity. V. Evolution of
463 reaction norm shape. *J. Evol. Biol.*, 6, 31-48.

bioRxiv preprint doi: https://doi.org/10.1101/2020.07.07.191320; this version posted July 8, 2020. The copyright holder for this preprint (which was not certified by peer review) is the author/funder, who has granted bioRxiv a license to display the preprint in perpetuity. It is made available under a CC-BY-NC-ND 4.0 International license.

464 Ghalambor, C.K., Hoke, K.L., Ruell, E.W., Fischer, E.K., Reznick, D.N. & Hughes, K.A.
465 (2015). Non-adaptive plasticity potentiates rapid adaptive evolution of gene
466 expression in nature. *Nature*, 525, 372-375.

467 Ghalambor, C.K., McKay, J.K., Carroll, S.P. & Reznick, D.N. (2007). Adaptive versus
468 non□adaptive phenotypic plasticity and the potential for contemporary adaptation in
469 new environments. *Funct. Ecol.*, 21, 394-407.

470 Gienapp, P., Teplitsky, C., Alho, J., Mills, J. & Merilä, J. (2008). Climate change and
471 evolution: disentangling environmental and genetic responses. *Mol. Ecol.*, 17, 167-
472 178.

473 Gilbert, S.F. (2000). *Developmental Biology, 6th edition*. Sinauer Associates, Sunderland,
474 MA.

475 Houle, D., Govindaraju, D. & Omholt, S. (2010). Phenomics: the next challenge. *Nature*
476 *Reviews Genetics*, 11, 855–866.

477 Lande, R. (2009). Adaptation to an extraordinary environment by evolution of phenotypic
478 plasticity and genetic assimilation. *J. Evol. Biol.*, 22, 1435-1446.

479 Legendre, P. & Legendre, L. (1998). *Numerical ecology*. 2nd English edition edn. Elsevier
480 Science, Amsterdam.

481 MacArthur, R.H. (1962). Some generalized theorems of natural selection. *Proc. Natl. Acad.*
482 *Sci. U.S.A.*, 48, 1893–1897.

483 Maharjan, R., McKenzie, C., Yeung, A. & Ferenci, T. (2013). The basis of antagonistic
484 pleiotropy in *hfq* mutations that have opposite effects on fitness at slow and fast
485 growth rates. *Heredity*, 110, 10-18.

486 Malerba, M.E., White, C.R. & Marshall, D.J. (2018). Eco□energetic consequences of
487 evolutionary shifts in body size. *Ecol. Lett.*, 21, 54-62.

488 Merilä, J. & Hendry, A.P. (2014). Climate change, adaptation, and phenotypic plasticity: the
489 problem and the evidence. *Evol. Appl.*, 7, 1-14.

bioRxiv preprint doi: https://doi.org/10.1101/2020.07.07.191320; this version posted July 8, 2020. The copyright holder for this preprint (which was not certified by peer review) is the author/funder, who has granted bioRxiv a license to display the preprint in perpetuity. It is made available under a CC-BY-NC-ND 4.0 International license.

490 Oksanen, J., Blanchet, F.G., Friendly, M., Kindt, R., Legendre, P., McGlinn, D. *et al.* (2019).
491 vegan: Community Ecology Package. http://CRAN.R-project.org/package=vegan
492 (accessed February 2019).

493 Oren, A. (2005). A hundred years of *Dunaliella* research: 1905–2005. *Saline Systems*, 1, 2.

494 Ozgul, A., Childs, D.Z., Oli, M.K., Armitage, K.B., Blumstein, D.T., Olson, L.E. *et al.*
495 (2010). Coupled dynamics of body mass and population growth in response to
496 environmental change. *Nature*, 466, 482-485.

497 Papageorgiou, G.C. (2004). Fluorescence of photosynthetic pigments in vitro and in vivo. In:
498 *Chlorophyll a fluorescence: A signature of photosynthesis. Advances in photosynthesis*
499 *and respiration.* (eds. Papageorgiou, GC & Govindjee). Springer Dordrecht, pp. 43-
500 63.

501 Pelletier, F., Clutton-Brock, T., Pemberton, J., Tuljapurkar, S. & Coulson, T. (2007). The
502 evolutionary demography of ecological change: linking trait variation and population
503 growth. *Science*, 315, 1571-1574.

504 Pendergrass, S.A., Brown-Gentry, K., Dudek, S., Frase, A., Torstenson, E.S., Goodloe, R. *et*
505 *al.* (2013). Phenome-wide association study (PheWAS) for detection of pleiotropy
506 within the Population Architecture using Genomics and Epidemiology (PAGE)
507 Network. *PLoS Genet.*, 9, e1003087.

508 Peres-Neto, P.R., Legendre, P., Dray, S. & Borcard, D. (2006). Variation partitioning of
509 species data matrices: estimation and comparison of fractions. *Ecology*, 87, 2614-
510 2625.

511 Phillimore, A.B., Leech, D.I., Pearce□Higgins, J.W. & Hadfield, J.D. (2016). Passerines may
512 be sufficiently plastic to track temperature□mediated shifts in optimum lay date.
513 *Global Change Biol.*, 22, 3259-3272.

514 Proulx, S.R., Dey, S., Guzella, T. & Teotónio, H. (2019). How differing modes of non-genetic
515 inheritance affect population viability in fluctuating environments. *Ecol. Lett.*, 22,
516 1767-1775.

517 R Core Team (2019). R: A language and environment for statistical computing. R Foundation
518 for Statistical Computing Vienna, Austria.

bioRxiv preprint doi: https://doi.org/10.1101/2020.07.07.191320; this version posted July 8, 2020. The copyright holder for this preprint (which was not certified by peer review) is the author/funder, who has granted bioRxiv a license to display the preprint in perpetuity. It is made available under a CC-BY-NC-ND 4.0 International license.

519 Reed, T.E., Waples, R.S., Schindler, D.E., Hard, J.J. & Kinnison, M.T. (2010). Phenotypic
520 plasticity and population viability: the importance of environmental predictability.
521 *Proc. R. Soc. B*, 277, 3391-3400.

522 Rescan, M., Grulois, D., Ortega-Aboud, E. & Chevin, L.-M. (2020). Phenotypic memory
523 drives population growth and extinction risk in a noisy environment. *Nature Ecology*
524 *& Evolution*, 4, 193-201.

525 Sæther, B.-E., Visser, M.E., Grøtan, V. & Engen, S. (2016). Evidence for r-and K-selection in
526 a wild bird population: a reciprocal link between ecology and evolution. *Proc. R. Soc.*
527 *B*, 283, 20152411.

528 Scheiner, S.M. (1993). Genetics and evolution of phenotypic plasticity. *Annu. Rev. Ecol.*
529 *Syst.*, 24, 35-68.

530 Scheiner, S.M. & Yampolsky, L.Y. (1998). The evolution of *Daphnia pulex* in a temporally
531 varying environment. *Genetics Research*, 72, 25-37.

532 Schlichting, C.D. & Pigliucci, M. (1998). *Phenotypic evolution: a reaction norm perspective*.
533 Sinauer Associates Incorporated, MA.

534 Tufto, J. (2015). Genetic evolution, plasticity, and bet□hedging as adaptive responses to
535 temporally autocorrelated fluctuating selection: a quantitative genetic model.
536 *Evolution*, 69, 2034-2049.

537 Vedder, O., Bouwhuis, S. & Sheldon, B.C. (2013). Quantitative assessment of the importance
538 of phenotypic plasticity in adaptation to climate change in wild bird populations. *PLoS*
539 *Biol.*, 11, e1001605.

540 Wersto, R.P., Chrest, F.J., Leary, J.F., Morris, C., Stetler□Stevenson, M. & Gabrielson, E.
541 (2001). Doublet discrimination in DNA cell□cycle analysis. *Cytometry: The Journal*
542 *of the International Society for Analytical Cytology*, 46, 296-306.

543 West-Eberhard, M.J. (2003). *Developmental plasticity and evolution*. Oxford University
544 Press, USA.

545 Wigley, T., Smith, R. & Santer, B. (1998). Anthropogenic influence on the autocorrelation
546 structure of hemispheric-mean temperatures. *Science*, 282, 1676-1679.

bioRxiv preprint doi: https://doi.org/10.1101/2020.07.07.191320; this version posted July 8, 2020. The copyright holder for this preprint (which was not certified by peer review) is the author/funder, who has granted bioRxiv a license to display the preprint in perpetuity. It is made available under a CC-BY-NC-ND 4.0 International license.

Yvert, G., Ohnuki, S., Nogami, S., Imanaga, Y., Fehrmann, S., Schacherer, J. *et al.* (2013). Single-cell phenomics reveals intra-species variation of phenotypic noise in yeast. *BMC Systems Biology*, 7, 54.

bioRxiv preprint doi: https://doi.org/10.1101/2020.07.07.191320; this version posted July 8, 2020. The copyright holder for this preprint (which was not certified by peer review) is the author/funder, who has granted bioRxiv a license to display the preprint in perpetuity. It is made available under a CC-BY-NC-ND 4.0 International license.

551 **Table**

552 **Table 1. Partitioning of cell morphological variation.** The effect of all explanatory factors
553 and their interactions on multivariate patterns of cellular variation are quantified by their R^2
554 (proportion of total variation explained), and the significance of each R^2 was tested by
555 ANOVA-like permutation tests using 999 randomizations of the data (Legendre & Legendre
556 1998).

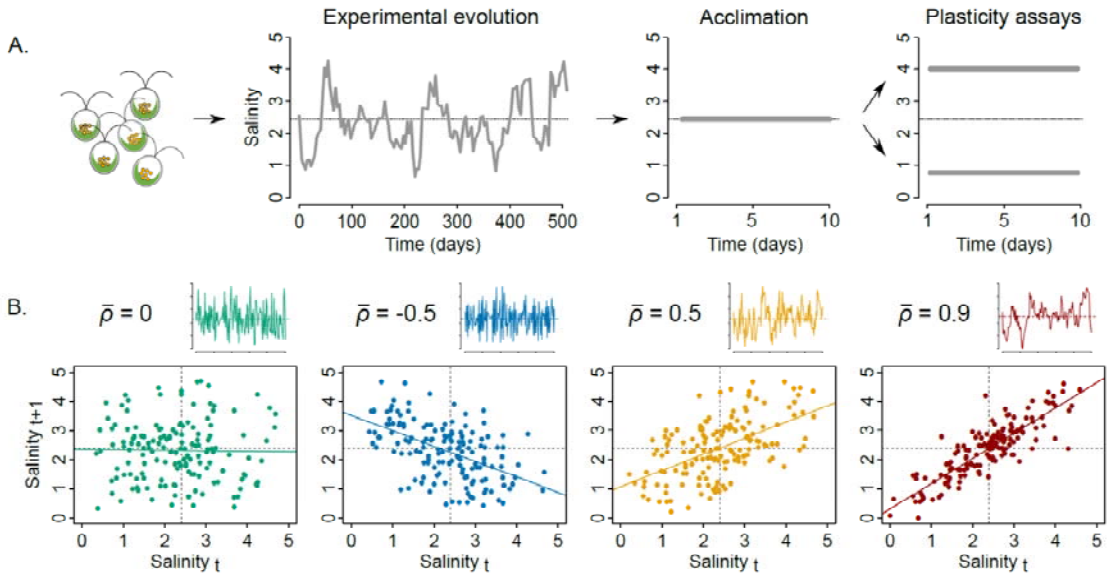
	Factors	df	Variance ($\times 10^{-3}$)	F	R^2	
Evolution in fluctuating salinity	Strain	2	2.407	2703.786	0.026	***
	Growth Rate	1	2.423	5443.078	0.026	***
	Day	9	10.446	2606.981	0.113	***
	Salinity	2	18.144	20376.765	0.196	***
	Predictability (ρ^2)	1	1.729	3883.617	0.019	***
	Salinity × ρ^2	2	1.384	1554.755	0.015	***
	Day × Salinity	18	3.764	469.737	0.041	***
	Day × Salinity × ρ^2	27	0.532	44.261	0.006	***
	Residual	116635	51.927		0.560	
Evolution in constant salinity	Strain	1	3.790	1048.620	0.042	***
	Growth Rate	1	1.856	513.564	0.021	***
	Day	9	15.808	485.962	0.176	***
	Salinity	1	22.000	6087.119	0.245	***
	Day × Salinity	9	3.226	99.183	0.036	***
	Residual	11880	42.938		0.479	

557 *** $P < 0.001$

bioRxiv preprint doi: https://doi.org/10.1101/2020.07.07.191320; this version posted July 8, 2020. The copyright holder for this preprint (which was not certified by peer review) is the author/funder, who has granted bioRxiv a license to display the preprint in perpetuity. It is made available under a CC-BY-NC-ND 4.0 International license.

558 **Figures legends**

559



560

561 **Fig. 1. Long-term evolution experiment under variable environmental predictability**. A.
562 The different steps of the experiment are illustrated. B. Examples of the four categories of
563 expected long-term temporal autocorrelation ( ). For each category, the small graph
564 represents the associated time series for a given population (same axes as in Fig. 1A), with
565 mean salinity shown as horizontal dotted line. The larger graphs represent the relationship
566 between subsequent salinities in these time series. Note that the expected autocorrelations =
567 -0.5 and = 0.5 lead to different magnitudes of salinity changes, but display the same
568 predictability of environmental changes (^{2} = 0.25).

bioRxiv preprint doi: https://doi.org/10.1101/2020.07.07.191320; this version posted July 8, 2020. The copyright holder for this preprint (which was not certified by peer review) is the author/funder, who has granted bioRxiv a license to display the preprint in perpetuity. It is made available under a CC-BY-NC-ND 4.0 International license.

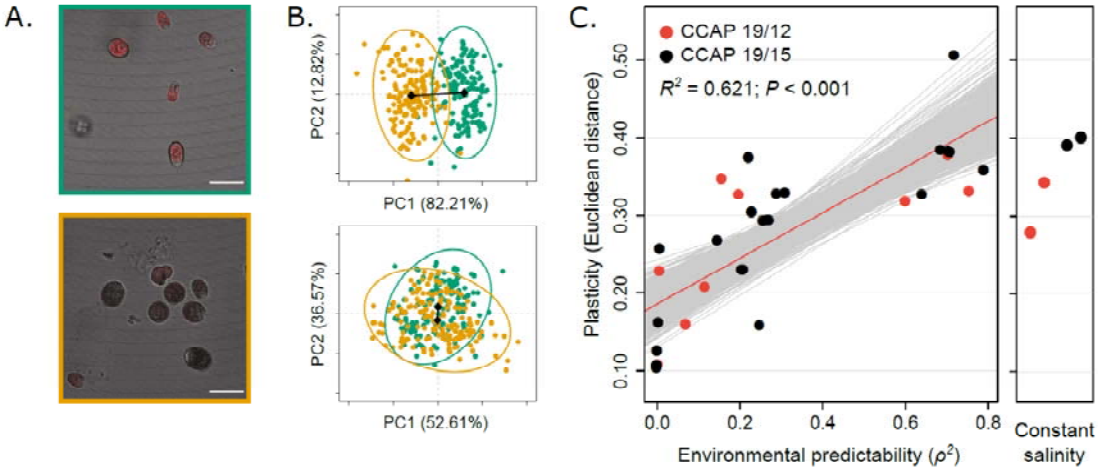
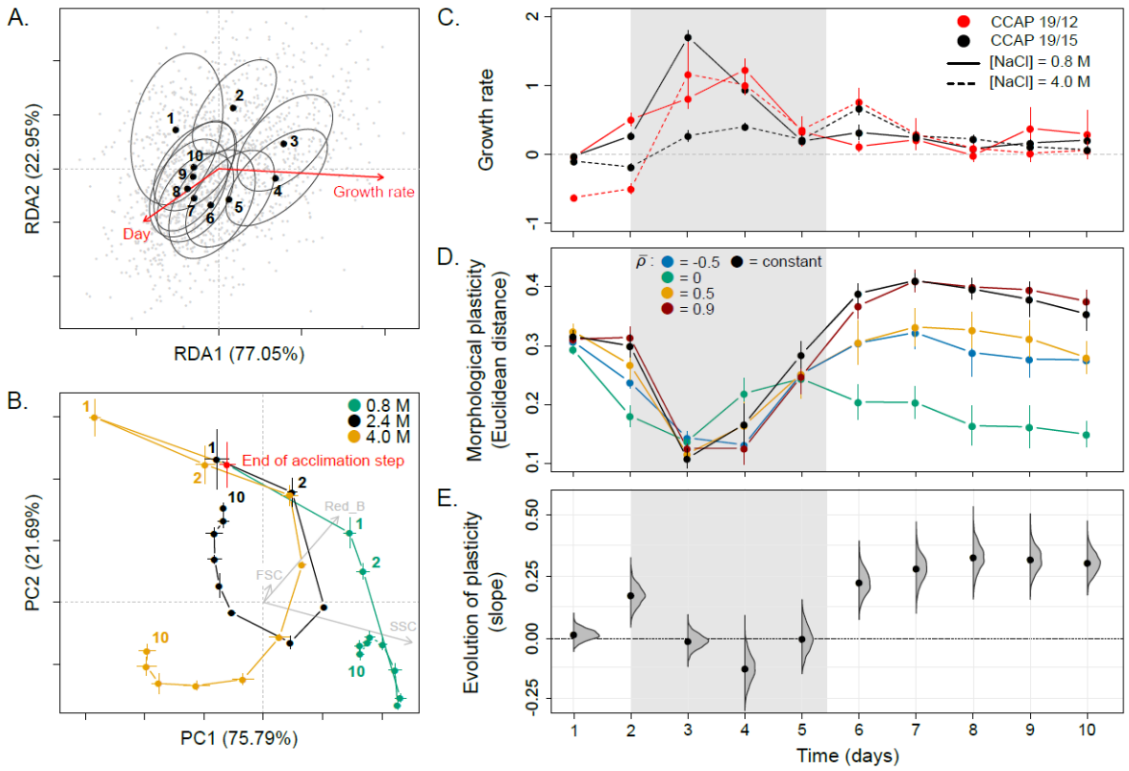


Fig. 2. Evolution of morphological plasticity in response to environmental predictability. A. Example of salinity-specific cell morphologies. Red zones in composite images represent chlorophyll fluorescence intensity and white bars give the scale (20µm) for populations in low (green) and high (orange) salinities. B. Morphological variation of cells after 10 days in low (green) and high (orange) salinities for populations that have evolved under predictable (upper graph) *vs* unpredictable (lower graph) environmental fluctuations. C. Evolution of the degree of plasticity at day 10. Standard error based on 1000 bootstraps are also plotted for each dot, but not visible. Red line is the regression slope, and the grey lines show 1000 regression slopes calculated on bootstrapped samples.

bioRxiv preprint doi: https://doi.org/10.1101/2020.07.07.191320; this version posted July 8, 2020. The copyright holder for this preprint (which was not certified by peer review) is the author/funder, who has granted bioRxiv a license to display the preprint in perpetuity. It is made available under a CC-BY-NC-ND 4.0 International license.



579

580 **Fig. 3. Evolution of plasticity along the ontogenic trajectory.** A. The ontogenic trajectory
581 of cell morphology for an isogenic population transferred to fresh medium with unchanged
582 salinity is shown as centroids (dots) and covariance matrices (ellipses) for each day. Arrows
583 indicate the RDA loadings. B. Trajectories of four isogenic populations from the same
584 evolved line in three different salinities. PC loadings of flow cytometry measurements (grey
585 arrows) were rescaled by dividing them by 20 to facilitate graphical representation. C. Per
586 capita population growth rate per day, across all evolved lines. D. Temporal variation in the
587 degree of phenotypic plasticity of the four treatments of expected long-term temporal
588 autocorrelation ($\overline{\rho}$), and populations that evolved in constant salinity (black). E: Evolution of
589 plasticity along the ontogeny. The mean slope of the regression of the degree of plasticity
590 (Euclidian distance between environments) against environmental predictability (ρ^2) is shown
591 for each day post transfer to a new salinity. Density plots represent slopes estimated on 1000
592 bootstrapped samples of the raw data (same as grey lines in Fig. 2C for day 10). For C to E,
593 the grey dashing delimits the phase with highest growth rate. Means with their standard errors
594 are represented as dots and error bars respectively.

bioRxiv preprint doi: https://doi.org/10.1101/2020.07.07.191320; this version posted July 8, 2020. The copyright holder for this preprint (which was not certified by peer review) is the author/funder, who has granted bioRxiv a license to display the preprint in perpetuity. It is made available under a CC-BY-NC-ND 4.0 International license.

Supplementary Material 1: Comparison of flow cytometry vs confocal microscopy methods to assess cells morphology

We carried out microscopy images analyses on a small subset of populations, to confirm the accuracy of flow cytometry for assessing cell morphology.

Methods: As for the main plasticity assay, we first acclimatized four randomly chosen evolved populations to the mean salinity ([NaCl] = 2.4 M) during 10 days. We then transferred each of them to low ([NaCl] = 0.8 M) and high ([NaCl] = 4.0 M) salinity for 10 others days. We finally measured cell morphology using flow cytometry and dragonfly confocal microscopy.

Dragonfly confocal microscopy: We sampled ~40µL of cultures from each condition (n = 8, for 4 populations in 2 salinities), and scanned them on a Dragonfly (COM4) spinning disk confocal microscope with 2 cameras EMCCD iXon888 Life (Oxford Instrument - Andor). A total of 100 images was taken under both transmission and confocal fluorescence modes, to assess cells shape and chlorophyll content, respectively. Wavelengths excitation and emission were at 488 nm and 700/775 nm, respectively, for confocal fluorescence.

We then used the automatic image analysis software Fiji (Schindelin *et al.* 2012) to characterize cells morphology. First, we used the function *Analyze Particles* to isolate cells in each picture, and manually validate each detected particle as an actual *D. salina* cell. For each particle, we then recorded morphological descriptors including the area and aspect ratio (AR: major/minor axis), the average gray - sum of the gray values of all the pixels in the selection divided by the number of pixels (Grey_Int and Grey_sd for mean and standard error respectively) - for the transmission mode, and fluorescence intensity (Fluo_Int and Fluo_sd for mean and standard error respectively) within the selection.

Flow cytometry: We passed a 150 µL sample of each condition through flow cytometry, using the same method as described in the main text. We then randomly selected 30 events characterized as alive *Dunaliella salina* cells per condition, to keep a balanced sampled size with the microscopy dataset. We then used FSC, SSC and Red-B values, followed by light

bioRxiv preprint doi: https://doi.org/10.1101/2020.07.07.191320; this version posted July 8, 2020. The copyright holder for this preprint (which was not certified by peer review) is the author/funder, who has granted bioRxiv a license to display the preprint in perpetuity. It is made available under a CC-BY-NC-ND 4.0 International license.

signal correction using Guava® EasyCheck™ kit calibrating beads, to assess cells morphology.

Statistical analyses: We tested the concordance of the morphospaces obtained by using the two methods, as proposed by Wang *et al.* (2010). We first carried out independent principal component analyses of morphology for flow cytometry and microscopy. We thereafter extracted the centroids on PCA plot for each group of cells, characterized by their population and salinity. Finally, we aligned the centroids' PCA coordinates of flow cytometry morphospace with the microscopy ones using a Procrustean superimposition approach (Gower 1975; Legendre & Legendre 1998). The degree of concordance between the ordinations was assessed with a correlation-like statistic *r*-PROTEST(Jackson 1995), derived from the symmetric sum of squares, where 1 and 0 denote a perfect vs totally absent concordance, respectively. The significance of this correlation was tested by permutation, using 999 randomizations against the null hypothesis that there is no concordance between the two ordinations (Jackson 1995).

Supplementary Information references:

Gower, J.C. (1975). Generalized Procrustes analysis. *Psychometrika*, 40, 33-51.

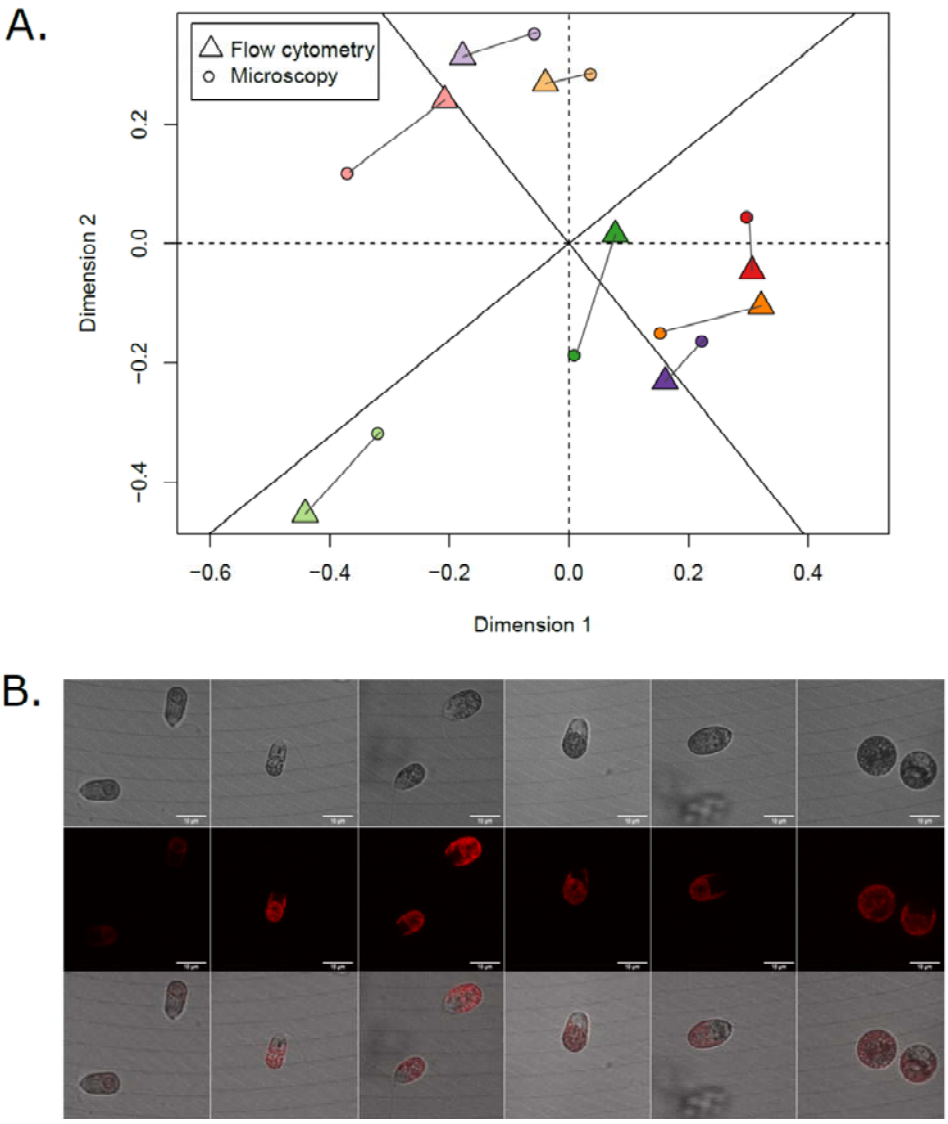
Jackson, D.A. (1995). PROTEST: a PROcrustean Randomization TEST of community environment concordance. *Ecoscience*, 2, 297-303.

Legendre, P. & Legendre, L. (1998). *Numerical ecology*. 2nd English edition edn. Elsevier Science, Amsterdam.

Schindelin, J., Arganda-Carreras, I., Frise, E., Kaynig, V., Longair, M., Pietzsch, T. *et al.* (2012). Fiji: an open-source platform for biological-image analysis. *Nat. Methods*, 9, 676-682.

Wang, C., Szpiech, Z.A., Degnan, J.H., Jakobsson, M., Pemberton, T.J., Hardy, J.A. *et al.* (2010). Comparing spatial maps of human population-genetic variation using Procrustes analysis. *Statistical Applications in Genetics and Molecular Biology*, 9.

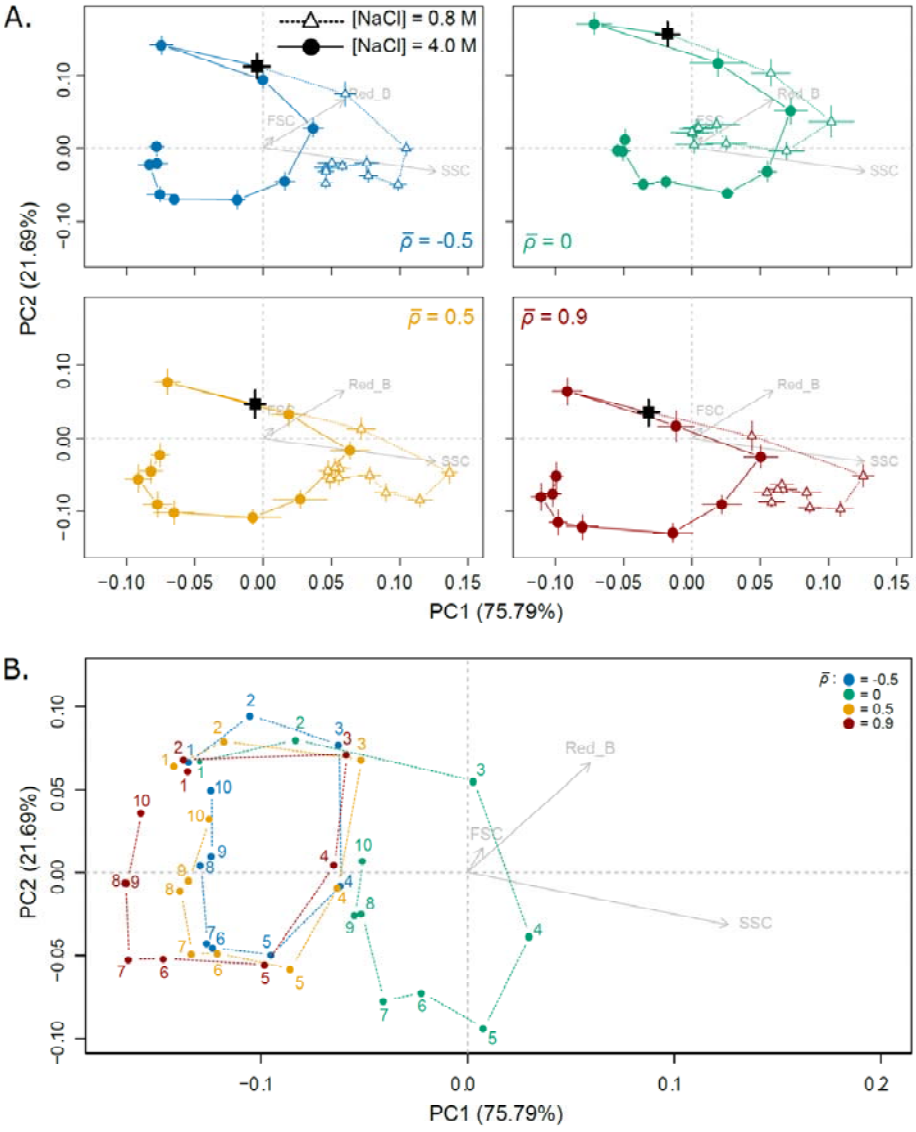
bioRxiv preprint doi: https://doi.org/10.1101/2020.07.07.191320; this version posted July 8, 2020. The copyright holder for this preprint (which was not certified by peer review) is the author/funder, who has granted bioRxiv a license to display the preprint in perpetuity. It is made available under a CC-BY-NC-ND 4.0 International license.



650

651 **Supp. Fig. S1. Comparison of flow cytometry vs confocal microscopy methods to assess**
652 **cells morphology.** A. Procrustes errors between PCAs performed on flow cytometry
653 (triangle) and confocal microscopy (circle) parameters. Each color represent the centroids of a
654 given population, with lighter vs darker colors for low (0.8 M) vs high (4.0 M) salinity,
655 respectively. B. Example of cell morphology. Images were taken using a dragonfly confocal
656 microscope, under the transmission (first line) and confocal in fluorescence (second line)
657 acquisitions respectively, and a composite of both acquisitions (third line, similar to Fig. 2B
658 in the main text). White scale bar represents 10µm.

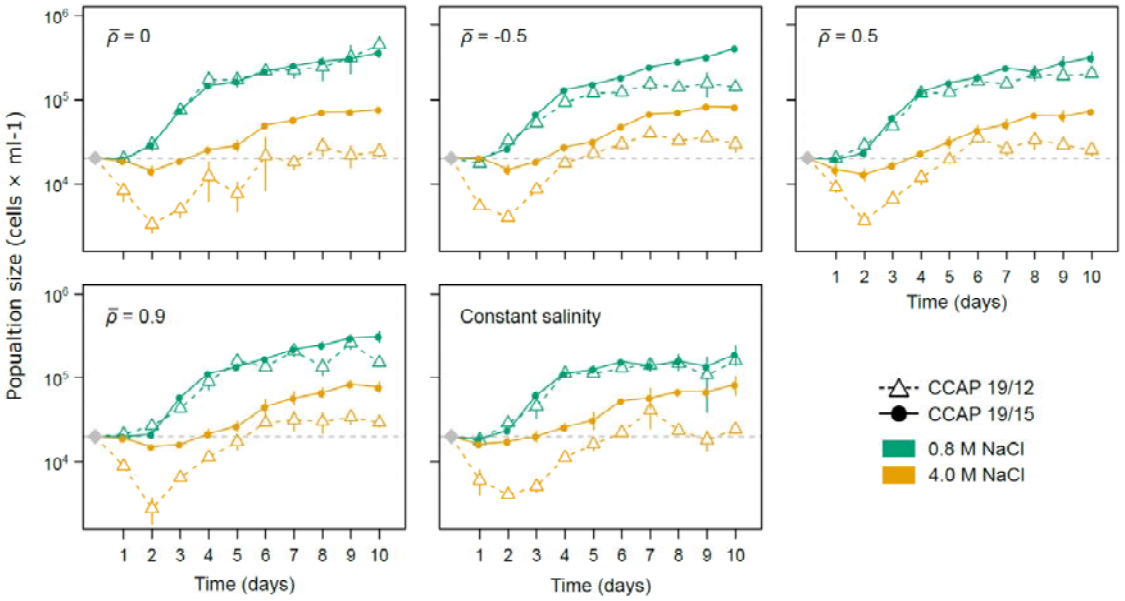
bioRxiv preprint doi: https://doi.org/10.1101/2020.07.07.191320; this version posted July 8, 2020. The copyright holder for this preprint (which was not certified by peer review) is the author/funder, who has granted bioRxiv a license to display the preprint in perpetuity. It is made available under a CC-BY-NC-ND 4.0 International license.



659

660 **Supp. Fig. S2. Ontogenetic trajectories and dynamics of plasticity over time.** A.
661 Morphological trajectories in two salinities for each autocorrelation treatment ($\bar{\rho}$). Mean cell
662 morphologies with their standard errors, per day and salinity, are calculated by averaging over
663 lines belonging to the same targeted $\bar{\rho}$, and represented along the two first PCA axes. Vectors
664 of PC loadings of response variables (FSC, SSC and Red_B grey arrows) were divided by 20
665 to facilitate graphical representation. Black squares represent cell morphology at the end of
666 acclimation step. B. Trajectories of plasticity over time. Morphological differences between
667 salinities for each treatments were computed as vector at high salinity *minus* the one at low
668 salinity, for each day (number).

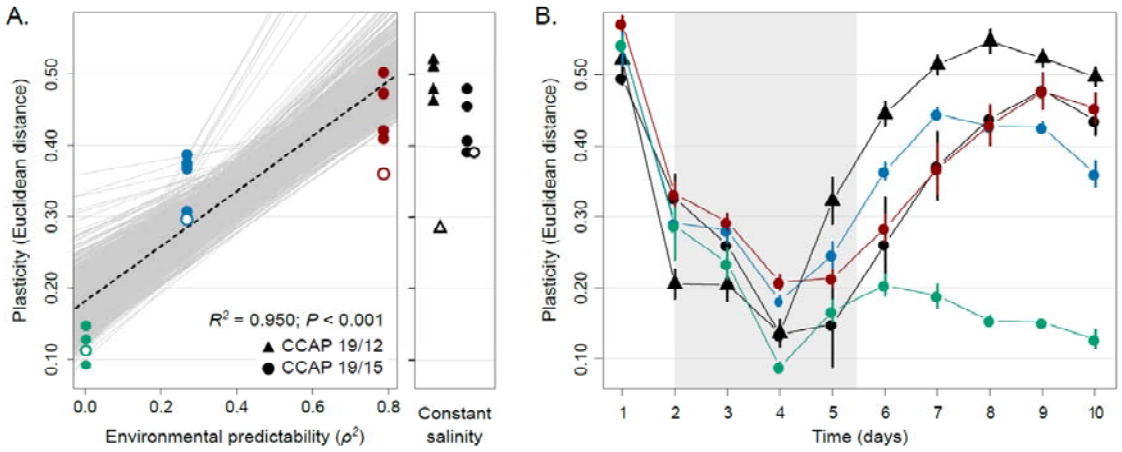
bioRxiv preprint doi: https://doi.org/10.1101/2020.07.07.191320; this version posted July 8, 2020. The copyright holder for this preprint (which was not certified by peer review) is the author/funder, who has granted bioRxiv a license to display the preprint in perpetuity. It is made available under a CC-BY-NC-ND 4.0 International license.



669

670 **Supp. Fig. S3. Population dynamics in low and high salinities.** For each evolutionary
671 treatment (temporal autocorrelation ($\bar{\rho}$) or constant salinity at [NaCl] = 2.4M), mean
672 population size (cells × ml^{-1}) with their standard errors, per day and salinity, were calculated
673 by averaging over lines belonging to the same strain. Grey diamond is the expected initial
674 population size (2×10^4 cells × ml^{-1}) inoculated in the new salinity at the beginning of the
675 plasticity assay, and day 1 was measure 4h after this salinity change.

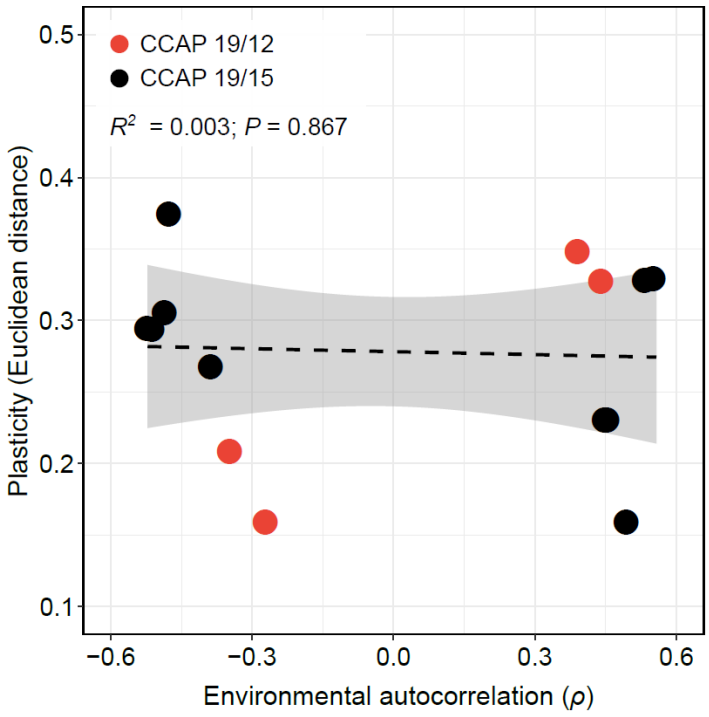
bioRxiv preprint doi: https://doi.org/10.1101/2020.07.07.191320; this version posted July 8, 2020. The copyright holder for this preprint (which was not certified by peer review) is the author/funder, who has granted bioRxiv a license to display the preprint in perpetuity. It is made available under a CC-BY-NC-ND 4.0 International license.



676

677 **Supp. Fig. S4. Analyses of isogenic populations.** A. Evolution of plasticity at day 10.
678 Isogenic populations were founded from a single cell from tree different evolved lines under ρ
679 = -0.022 (green), ρ = -0.522 (blue) and ρ = 0.889 (red) and two strain (CCAP 19/12 as triangle
680 and CCAP 19/15 as circle) from constant environment. The degree of plasticity of
681 populations, measured as the Euclidian distance of mean cell morphology between low and
682 high salinities, is plotted against the predictability ρ^2 of environmental fluctuations of these
683 populations that have experienced during experimental evolution. Standard error based on
684 1000 bootstraps are also plotted, but not visible. The regression slope is represented as red
685 line, and the grey lines encompass 1000 regression slopes calculated for each bootstrap. The
686 panel on the right shows plasticity in populations that evolved under constant salinity,
687 corresponding to the mean of fluctuating treatments. Variation partitioning revealed
688 significant morphological differences among isogenic populations founded from a given
689 evolved lines (R^2 = 0.009; P < 0.001), but those remained smaller than morphological
690 variation among different evolved lines (R^2 = 0.051; P < 0.001), when controlling for the
691 effect of salinity, day, and their interaction on the total variation. Filled and open symbols
692 represent isogenic populations and the evolved lines they come from, respectively. B.
693 Temporal variation in the degree of phenotypic plasticity. For each population, Euclidean
694 distances were computed between mean cell morphologies in [NaCl] = 0.8M vs 4.0M. Means
695 and standard errors were assessed from 4 isogenic populations for each evolved lines.

bioRxiv preprint doi: https://doi.org/10.1101/2020.07.07.191320; this version posted July 8, 2020. The copyright holder for this preprint (which was not certified by peer review) is the author/funder, who has granted bioRxiv a license to display the preprint in perpetuity. It is made available under a CC-BY-NC-ND 4.0 International license.



696

697 **Supp. Fig. S5. Influence of the magnitude of environmental transitions for a given**
698 **environmental predictability.** The degree of plasticity of populations, measured as the mean
699 Euclidean distance of cell morphology after 10 days in low vs high salinities, is plotted
700 against the environmental autocorrelation ($\bar{\rho}$). Negative and positive autocorrelation displayed
701 the same environmental predictability ($\bar{\rho}^2 = 0.25$), but differed in the intensity of
702 environmental changes between two successive transfers. The regression slope is also
703 represented as black dashed line, and the shaded region shows the 95% CI of this regression.